



Flutter of rectangular simply supported plates at low supersonic speeds



Sergey Shitov, Vasily Vedeneev*

Steklov Mathematical Institute of Russian Academy of Sciences, 8, Gubkina str., Moscow, Russia

ARTICLE INFO

Keywords:

Panel flutter
Single mode flutter
Single degree of freedom flutter
Rectangular plate

ABSTRACT

Aeroelastic instability of skin panels, known as panel flutter, can occur in the form of coupled-mode or single-mode flutter. While the first type of flutter usually occurs in one eigenmode (composed of the first and the second natural modes in vacuum) and yields well-studied nonlinear limit cycle oscillations, the single mode flutter can occur in several simultaneously growing eigenmodes, leading to complex nonlinear panel dynamics, including different co-existing limit cycles, periodic and non-periodic higher-mode oscillations. Structural nonlinearity and linear aeroelastic growth mechanism play the major role in this dynamic.

While the linear panel flutter boundaries in the two-dimensional formulation have been studied in detail, there are only few investigations of the boundaries in the three-dimensional case. Since the linear growth mechanism plays an essential role in nonlinear oscillations, its comprehensive study is an important step toward understanding of complex dynamics of skin panels in the three-dimensional case. In this paper, we investigate the flutter boundaries of rectangular panels simply supported at all edges, and use potential flow theory to calculate the unsteady pressure. The problem is considered in two formulations: a series of rectangular plates, attached to each other, and a single rectangular plate. Flutter boundaries of the first four modes are calculated, and their transformations with the change of the spanwise plate width are studied in detail.

1. Introduction

Panel flutter is a phenomenon of self-exciting skin panel vibrations in flight vehicles moving at high speeds. Unlike wing flutter, usually it does not immediately yield the destruction of panels, but results in fatigue damage and rapidly decreases their lifetime. Although panel flutter was first observed during WWII, the first essential theoretical studies were conducted a decade later (Movchan, 1956, 1957). In these works, the Kirchhoff–Love model for panel dynamics and piston theory for unsteady flow pressure (Iliushin, 1956; Ashley and Zartarian, 1956) were used. During the following decades, the panel flutter problem was studied in more complex formulations (Bolotin, 1963; Grigolyuk et al., 1965; Dugundji, 1966; Dowell, 1974; Novichkov, 1978; Mei et al., 1999; Algazin and Kiiko, 2006). In most of these works, the ‘elastic’ part of the problem was subject to complication: multi-layered and composite panels, non-flat shells, geometrical and material nonlinearity, and complex material properties, including viscoelastic materials, shape memory alloys, and piezoelectric materials (Kiiko and Pokazeev, 2005; Duan et al., 2003; Zhou et al., 1995). The ‘aerodynamic’ part of the problem was not changed: the piston theory was employed.

The linearised unsteady pressure of inviscid gas, acting on the oscillating plate (i.e., the potential flow theory), has the form of an

* Corresponding author.

E-mail addresses: shitov@gmail.com (S. Shitov), vasily@vedeneev.ru (V. Vedeneev).

integral operator of a combination of the plate deflection and its spatial derivative, with a kernel consisting of special functions (Miles, 1959). In the limit of $M \rightarrow \infty$, this expression yields the piston theory formula; however, for Mach numbers $M < 2$, the accuracy of the piston theory essentially drops, and it becomes totally invalid for $M < \sqrt{2}$. Substitution of the potential-flow expression for pressure into the plate equation yields an integro-differential eigenvalue problem, which, due to its complexity, was studied in just a few papers. Min-de (1958) and Ming-de (1984) gave a closed-form solution for the two-dimensional integro-differential problem, which makes the eigenvalue problem algebraic; however, the latter turned out to be so difficult that no attempts to solve it were made. Nelson and Cunningham (1956), Dowell (1974), and Yang (1975) solved the same integro-differential equation numerically through Galerkin and finite element methods for certain parameter values. It was noticed that, along with coupled-mode flutter, which occurs when the problem is solved through the piston theory, calculations at $1 < M < \sqrt{2}$ show the presence of another flutter type, namely, single mode (also called single-degree-of-freedom) flutter. Cunningham (1967) studied flutter of rectangular simply supported and clamped panels at $M=1.3$ through the potential flow theory and showed that single mode flutter is also present in the three-dimensional problem, but disappears if the plate becomes sufficiently narrow in the spanwise direction. Dowell (1974) also studied nonlinear limit cycle oscillations by combining a nonlinear von Karman plate model with linearised potential flow theory, and observed pure first-mode oscillations at $1 < M < \sqrt{2}$.

Later the problem of panel flutter was numerically analysed through more complex aerodynamic models, which take into account aerodynamic nonlinearity, or shear flow aerodynamics, or both. Bendiksen and Davis (1995), Bendiksen and Seber (2008), Mei et al. (2014), and Shishaeva et al. (2015) studied transonic and supersonic flutter in inviscid flow, while Dowell (1971, 1973), Gordnier and Visbal (2002), Hashimoto et al. (2009), Visbal (2014), and Alder (2015, 2016) investigated flutter in a viscous flow.

A completely different approach was used by Vedeneev (2005), who analytically studied the two-dimensional panel flutter problem with the potential flow aerodynamics through an asymptotic method of global instability (Kulikovskii, 1966) for sufficiently long plates. It was strictly proved that single-mode flutter exists, and the physical mechanism of perturbation growth was revealed. The important feature proved is that the single-mode flutter cannot be obtained if the piston theory is used (although, as was recently shown by Ganji and Dowell (2016), higher-order expansions of the potential flow theory in the oscillation frequency yield correct results at $M < \sqrt{2}$, while the piston theory, being the first-term expansion, is just wrong at these M). Later Vedeneev (2012, 2013a) solved this problem numerically and calculated the stability boundaries of the first six eigenmodes. Flutter region consists of coupled mode flutter region and single mode flutter regions in various modes; the single mode flutter is dominant at low supersonic Mach numbers and short plates. It was shown in a closed form (Vedeneev, 2007, 2013b) and confirmed numerically (Shishaeva et al., 2015) that the multiplicity of linearly growing eigenmodes at small supersonic speeds yields the complex nonlinear dynamics of the panel, which includes the co-existence of regular limit cycles and cycles with internal 1:2 resonance, higher-mode limit cycles, and non-periodic oscillations.

The asymptotic method of Kulikovskii (1966) was also effective in the investigation of the boundary layer influence: Vedeneev (2013c) and Bondarev and Vedeneev (2016) conducted a general study of the boundary layer effect on panel flutter for arbitrary boundary layer profiles and showed that this effect is very different for boundary layers over convex and concave walls, and can be essentially destabilising for certain flow conditions.

The three-dimensional flutter problem for rectangular panels of large lengths with potential flow aerodynamics was studied by Vedeneev (2006, 2010), using a modified asymptotic method (Kulikovskii, 2006). Formulation of the problem for a numerical solution without additional assumption of large plate length is more complicated than the two-dimensional problem because the integration area in the integro-differential operator for the unsteady pressure becomes two-dimensional in the shape of a triangle (Miles, 1959). In this formulation, the problem was studied only by Dowell (1974), who investigated first-mode flutter for three plate aspect ratios at $M < \sqrt{2}$, and by Cunningham (1967), who considered several modes at Mach number $M=1.3$.

Thus, up to the present day, there is no general study of rectangular plate flutter in the potential-flow formulation for arbitrary aspect ratios and Mach numbers. The present paper aims to fill this gap, taking into account that linear plate dynamics is not only important by itself, but also plays a major role in the formation of nonlinear limit cycle oscillations (Shishaeva et al., 2015). We solve this problem in two formulations. First, we study a particular case; namely, we consider a series of simply supported rectangular plates attached to each other. In this case, the integral in the integro-differential eigenvalue problem becomes one-dimensional. Second, we solve the exact problem for an isolated plate and investigate the effect of the single panel. Flutter boundaries for the first four modes in the parameter space are studied in detail.

2. Formulation of the problem

We study the linear stability of an elastic plate which forms a part of the plane surface. One side of the surface is exposed to a supersonic gas flow, as shown in Fig. 1. The other side experiences constant pressure so that the undisturbed state of the plate is flat. The plate is simply supported along all edges. We consider two plate configurations. In the first one, the plate is an infinite strip of the chordwise length L_{xw} , which is periodically simply supported with the spanwise period L_{yw} (Fig. 1a). This also can be represented as an infinite series of rectangular plates of $L_{xw} \times L_{yw}$ size attached to each other. Obviously, due to connections between spans, they are all either simultaneously stable or unstable. In the second configuration, the plate is a single rectangle of $L_{xw} \times L_{yw}$ size (Fig. 1b).

While the plate equation and boundary conditions in both configurations are the same, the aerodynamics are different. In the first case, each rectangular segment is affected by surrounding segments; in the second case it is not. We will show that in the first

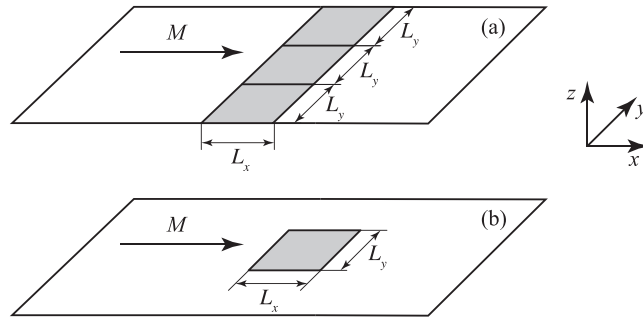


Fig. 1. Gas flow over (a) series of plates and (b) single plate, mounted into a rigid plane.

configuration the unsteady pressure is expressed as a one-dimensional integro-differential operator of the plate deflection, while in the second case this operator is two-dimensional. That is why the second case is more computationally expensive.

Introduce the coordinate system as shown in Fig. 1. The gas flows along the x -axis, while z -axis is normal to the plate surface. The bending stiffness of the plate is D_w , thickness is h , and the material density is ρ_m . In-plane tension of the plate and body forces are neglected.

The gas is inviscid (the boundary layer is neglected) and perfect, the flow is adiabatic. Its undisturbed density and speed of sound are ρ_0 and a_0 . The gas flows in the half-space $z > 0$ with constant supersonic speed U_0 .

The Kirchhoff–Love equation of motion for an elastic plate in a gas flow and simply supported boundary conditions are as follows:

$$\begin{aligned} \rho_m h \frac{\partial^2 w}{\partial t^2} + D_w \Delta^2 w + p &= 0, \quad 0 < x < L_{xw}, \quad 0 < y < L_{yw}, \\ w = \frac{\partial^2 w}{\partial x^2} = 0, \quad x = 0, L_{xw}, \quad w = \frac{\partial^2 w}{\partial y^2} = 0, \quad y = 0, L_{yw}, \end{aligned} \tag{1}$$

where Δ is the two-dimensional Laplace operator and $w(x, y, t)$ is the plate deflection. Linearised potential flow theory yields the following expression for the pressure perturbation $p(x, y, t)$ acting on the plate, through the perturbation of the flow potential $\varphi(x, y, z, t)$:

$$p(x, y, t) = -\rho_0 \left(\frac{\partial}{\partial t} + U_0 \frac{\partial}{\partial x} \right) \varphi(x, y, 0, t). \tag{2}$$

Linearised wave equation and boundary conditions (radiation as $z \rightarrow +\infty$ and impenetrability at the plate surface) for small flow perturbations have the form

$$\left(\frac{\partial}{\partial t} + U_0 \frac{\partial}{\partial x} \right)^2 \varphi - a_0^2 \frac{\partial^2 \varphi}{\partial x^2} - a_0^2 \frac{\partial^2 \varphi}{\partial y^2} - a_0^2 \frac{\partial^2 \varphi}{\partial z^2} = 0, \quad z > 0 \tag{3}$$

$$\left(\frac{\partial \varphi}{\partial x}, \frac{\partial \varphi}{\partial y}, \frac{\partial \varphi}{\partial z} \right) \rightarrow 0 \text{ as } z \rightarrow +\infty \text{ along rays } z = \frac{x - x_0}{\sqrt{M^2 - 1}} \tag{4}$$

$$\frac{\partial \varphi}{\partial z} = \frac{\partial w}{\partial t} + U_0 \frac{\partial w}{\partial x}, \quad z = 0, \quad (x, y) \in S; \quad \frac{\partial \varphi}{\partial z} = 0, \quad z = 0, \quad (x, y) \notin S, \tag{5}$$

where S is the plate surface: $x \in [0; L_{xw}]$ in the first configuration and $(x, y) \in [0; L_{xw}] \times [0; L_{yw}]$ in the second. The radiation condition (4), which represents decay of perturbations along characteristics $z = (x - x_0)/\sqrt{M^2 - 1}$ at fixed t and y , is satisfied only for growing perturbations.

In order to nondimensionalise the system, we take a_0 , ρ_0 , and h as dimensionally independent scales. Then

$$x = \tilde{x}h, \quad y = \tilde{y}h, \quad z = \tilde{z}h, \quad t = \tilde{t} \frac{h}{a_0}, \quad \varphi = \tilde{\varphi} a_0 h, \quad w = \tilde{w}h$$

where tildes represent dimensionless variables. Dimensionless parameters are expressed as follows:

$$D = \frac{D_w}{a_0^2 \rho_m h^3}, \quad L_x = \frac{L_{xw}}{h}, \quad L_y = \frac{L_{yw}}{h}, \quad M = \frac{U_0}{a_0}, \quad \mu = \frac{\rho_0}{\rho_m}, \tag{6}$$

where D , L_x , and L_y are dimensionless stiffness, length, and width of the plate, respectively, and M and μ are Mach number and dimensionless gas density, respectively. Dimensionless dynamic pressure and mass ratio, not used in this study but widely used in aeroelasticity, can be expressed through parameters (6) as

$$\lambda^* = \frac{\rho_0 U_0^2 L_{xw}^3}{D_w} = \frac{\mu M^2 L_x^3}{D}, \quad \mu^* = \frac{\rho_0 L_{xw}}{\rho_m h} = \mu L_x.$$

Below we will omit tildes, assuming that all variables are dimensionless.

The stability of the plate is determined by the stability of its eigenmodes; that is why we will consider small perturbations in the form

$$w(x, y, t) = W(x, y)e^{-i\omega t}, \quad \varphi(x, y, z, t) = \Phi(x, y, z)e^{-i\omega t}. \tag{7}$$

Substituting (7) into the nondimensionalised system (1)–(5), we obtain the closed system of dimensionless equations for perturbations consisting of the plate equation:

$$\begin{aligned} D\Delta^2 W - \omega^2 W + P &= 0, \quad 0 < x < L_x, \quad 0 < y < L_y, \\ P &= -\mu \left(-i\omega + M \frac{\partial}{\partial x} \right) \Phi(x, y, 0), \\ W = \frac{\partial^2 W}{\partial x^2} = 0, \quad x = 0, \quad L_x, \quad W = \frac{\partial^2 W}{\partial y^2} = 0, \quad y = 0, \quad L_y, \end{aligned} \tag{8}$$

and the flow equation

$$\begin{aligned} \left(-i\omega + M \frac{\partial}{\partial x} \right)^2 \Phi - \frac{\partial^2 \Phi}{\partial x^2} - \frac{\partial^2 \Phi}{\partial y^2} - \frac{\partial^2 \Phi}{\partial z^2} &= 0, \quad z > 0 \\ \left(\frac{\partial \Phi}{\partial x}, \frac{\partial \Phi}{\partial y}, \frac{\partial \Phi}{\partial z} \right) &\rightarrow 0 \text{ as } z \rightarrow +\infty \text{ along rays } z = \frac{x - x_0}{\sqrt{M^2 - 1}} \\ \frac{\partial \Phi}{\partial z} = -i\omega W + M \frac{\partial W}{\partial x}, \quad z = 0, \quad (x, y) \in S; \quad \frac{\partial \Phi}{\partial z} = 0, \quad z = 0, \quad (x, y) \notin S. \end{aligned} \tag{9}$$

The wave equation for the potential Φ with the boundary conditions (9) is solved in a closed form through Laplace transformation (Miles, 1959, §4.8), and the solution is as follows:

$$\begin{aligned} \Phi(x, y, 0) &= \iint_K -\frac{1}{\pi} \left(-i\omega W(\hat{x}, \hat{y}) + M \frac{\partial W(\hat{x}, \hat{y})}{\partial \hat{x}} \right) \exp \left(\frac{i\omega M}{\beta^2} (x - \hat{x}) \right) \\ &\times \frac{1}{\sqrt{(x - \hat{x})^2 - \beta^2 \hat{y}^2}} \cos \left(\frac{\omega}{\beta^2} \sqrt{(x - \hat{x})^2 - \beta^2 \hat{y}^2} \right) d\hat{x} d\hat{y} \end{aligned} \tag{10}$$

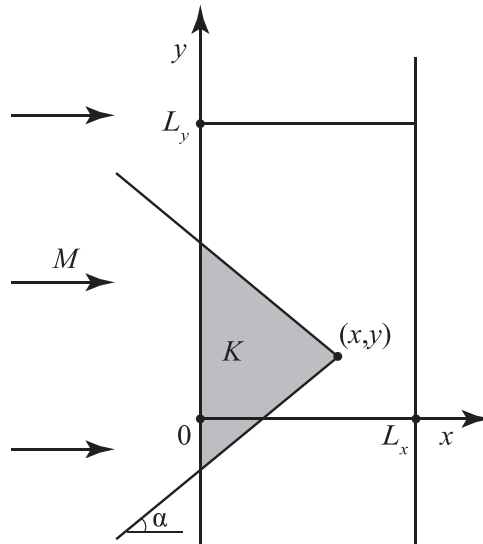


Fig. 2. Integration area K for obtaining unsteady pressure in the point (x,y) ; α is the Mach angle.

where K is a triangle that is an intersection of the reversed Mach cone with the vertex at the point (x,y) , with the plate (Fig. 2), $\beta = \sqrt{M^2 - 1}$.

Thus, the plate equation (8), after the substitution of (10), with simply supported boundary conditions, is an integro-differential eigenvalue problem for finding eigenvalues ω . This problem is solved numerically. The region of instability for the n -th mode in the parameter space is defined by the inequality $\text{Im } \omega_n > 0$. The plate is stable when each mode is damped.

3. Numerical procedure

3.1. Discretisation

We will use the Bubnov–Galerkin procedure for finding eigenvalues of the problem (8) with the potential Φ (10). The procedure described below is developed based on the method for the two-dimensional problem (Vedenev, 2012).

The plate deflection $W(x, y)$ is expressed as a superposition of basic functions, namely, mode shapes of the plate in vacuum:

$$W(x, y) = \sum_{k=1}^{N_x} \sum_{l=1}^{N_y} C_l^k \sin\left(\frac{k\pi x}{L_x}\right) \sin\left(\frac{l\pi y}{L_y}\right) = \sum_{k=1}^{N_x} \sum_{l=1}^{N_y} C_l^k W_k(x) W^l(y), \tag{11}$$

where C_l^k are unknown coefficients. Number the basic functions in the following manner:

$$T_{(l-1)N_x+k}(x, y) = W_k(x) W^l(y).$$

Then the sum (11) is rewritten as

$$W(x, y) = \sum_{m=1}^N C_m T_m(x, y), \tag{12}$$

where $N = N_x N_y$, $C_m = C_l^k$. For a given m , numbers k and l are restored as:

$$l = \left\lfloor \frac{m-1}{N_x} \right\rfloor + 1, \quad k = m - N_x(l-1), \tag{13}$$

where square brackets mean the floor function of the number. Substitute the sum (12) into the plate equation (8). Multiplying it in series by $(2/L_y)T_n(x, y)$, $n = 1 \dots N$, and integrating over the plate surface, we obtain a homogeneous system of linear algebraic equations with unknowns C_m and matrix $A(\omega)$:

$$A(\omega) = K - \frac{L_x \omega^2}{2} E + P(\omega). \tag{14}$$

Here E is the identity matrix; K is the diagonal stiffness matrix, which represents the plate properties, with coefficients

$$k_{mm} = \frac{L_x}{2} D \left[\left(\frac{k\pi}{L_x} \right)^4 + 2 \left(\frac{k\pi}{L_x} \right)^2 \left(\frac{l\pi}{L_y} \right)^2 + \left(\frac{l\pi}{L_y} \right)^4 \right],$$

where indices k and l are calculated through (13). P is the aerodynamic force matrix with coefficients p_{nm} :

$$p_{nm}(\omega) = \frac{2}{L_y} \int_0^{L_y} \int_0^{L_x} P(x, y, T_m, \omega) T_n(x, y) dx dy. \tag{15}$$

Thus, the frequency equation takes the form

$$\det A(\omega) = 0 \iff \det \left(K - \frac{L_x \omega^2}{2} E + P(\omega) \right) = 0. \tag{16}$$

3.2. Flow pressure for a plate oscillating in natural mode

In the matrix A (14), only the aerodynamic force matrix is calculated numerically, which requires the calculation of the unsteady aerodynamic pressure $P(x, y, T_m, \omega)$ for a plate oscillating in natural modes, and then integration (15). This section is devoted to the first problem, calculation of P .

3.2.1. Series of plates

Let us transform the expression (10) for the flow potential Φ in the case of the plate deflection $W(x, y)$ in the natural mode

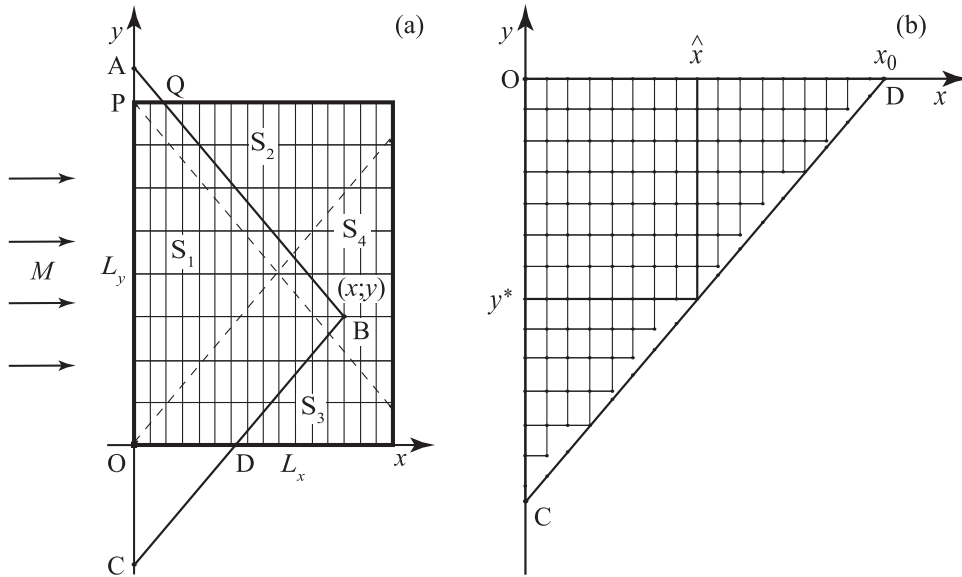


Fig. 3. Regions S_1 – S_4 of the plate (delimited by dashed lines), and the integration area for $(x, y) \in S_4$ (a) and integration over small triangles (b).

$$T_m(x, y) = W_k(x)W^l(y) = \sin(\alpha x)\sin(\lambda y), \quad \alpha = \frac{\pi k}{L_x}, \quad \lambda = \frac{\pi l}{L_y}, \tag{17}$$

for $-\infty < y < \infty$. The two-dimensional integral over the triangle K can be written as two iterated integrals with respect to x and y . Then the y -integral is calculated in a closed form. The resulting expression is as follows:

$$\Phi(x, y, 0) = -\frac{1}{\beta} \sin(\lambda y) \int_0^x (-i\omega \sin(\alpha \hat{x}) + M \alpha \cos(\alpha \hat{x})) \exp\left(\frac{i\omega M}{\beta^2}(x - \hat{x})\right) J_0(\xi) d\hat{x}, \tag{18}$$

where J_0 is the Bessel function of the first kind, $\xi = \sqrt{\omega^2 + (\beta\lambda)^2}(x - \hat{x})/\beta^2$.

Then, substituting (18) into the pressure expression (8), differentiating and grouping similar terms, we obtain:

$$P_{series}(x, y) = \sin(\lambda y) \times \left(\frac{\mu M}{\beta} (-i\omega \sin(\alpha x) + M \alpha \cos(\alpha x)) + \frac{\mu}{\beta^3} \times \int_0^x (-i\omega \sin(\alpha \hat{x}) + M \alpha \cos(\alpha \hat{x})) \exp\left(\frac{i\omega M}{\beta^2}(x - \hat{x})\right) \times (i\omega J_0(\xi) - M \sqrt{\omega^2 + (\beta\lambda)^2} J_1(\xi)) d\hat{x} \right) = W^l(y) P_x(x, W_k, \omega). \tag{19}$$

3.2.2. Single plate

Let the plate deflection, as before, be in the form (17) for $0 < y < L_y$, but the plate is now single, i.e., $W(x; y) = 0$ for $y < 0$ and $y > L_y$. Consider four regions of the plate, S_1, S_2, S_3 , and S_4 , as shown in Fig. 3a.

If the point $(x; y)$ belongs to the region S_1 , then the integration triangle K lies in the plate, and the expression for pressure is the same as for a series of plates:

$$P_{single}(x, y) = P_{series}(x, y),$$

where P_{series} is readily given by (19).

Consider the case of $(x, y) \in S_4$ (Fig. 3a). Then the integration triangle ABC (where B is the point (x, y)) does not fully belong to the plate; namely, integrals over triangles APQ and COD are zero, and that over the pentagon $PQBDO$ is not. Then the pressure is expressed through the potential (10), where $W(x, y)$ is given by (17), but the integration area is now the pentagon $PQBDO$. We add and subtract integrals over triangles APQ and COD in order to complete the integration area to the full triangle ABC , the integral over which is given by (19). Hence,

$$P_{single}(x, y) = P_{series}(x, y) - P_l(x; y) - P_r(x, y),$$

where P_l and R_r are calculated through the integrals (10) over triangles APQ and COD , respectively (indices ‘l’ and ‘r’ mean left and right triangles, as seen from the position of the flow).

Similarly, if the point (x,y) belongs to the region S_2 or S_3 , the pressure is given by

$$P_{single}(x, y) = P_{series}(x, y) - P_l(x, y), \quad P_{single}(x, y) = P_{series}(x, y) - P_r(x, y),$$

respectively.

Obviously, additional subtracted integrals over triangles APQ and COD for the points not belonging to S_1 represent the influence of the absence of plates surrounding the given plate, if compared to the case of the series of plates. Points of S_1 do not ‘feel’ this absence, because surrounding plates lie outside the reversed Mach cone, which is the region that influences the points belonging to S_1 .

Now, consider the calculation of the pressures P_l, P_r , starting with the right triangle, P_r . First, rewrite (10) in the form of iterated integrals by using (17):

$$\begin{aligned} \Phi_r(x, y) &= -\frac{1}{\pi} \int_0^{x_0(x,y)} V(\hat{x})f(x, \hat{x})F(x, y, \hat{x})d\hat{x}, \\ F(x, y, \hat{x}) &= \int_{y^*(x,y,\hat{x})}^0 \sin(\lambda\hat{y}) \frac{\cos(\omega\sqrt{(x-\hat{x})^2 - \beta^2(y-\hat{y})^2}/\beta^2)}{\sqrt{(x-\hat{x})^2 - \beta^2(y-\hat{y})^2}} d\hat{y}, \end{aligned} \tag{20}$$

where $x_0(x, y) = x - \beta y$, $y^*(x, y, \hat{x}) = y - (x - \hat{x})/\beta$ (Fig. 3b), and the following notations are introduced:

$$V(\hat{x}) = (-i\omega\sin(\alpha\hat{x}) + M\alpha\cos(\alpha\hat{x})), \quad f(x, \hat{x}) = \exp\left(\frac{i\omega M}{\beta^2}(x-\hat{x})\right).$$

The main difficulty in the direct integration of (20) is the singularity of the integrand in F at $\hat{y} = y^*$. Since it is integrable, we will first remove it by changing variables. Namely, introduce variable η as follows:

$$\eta = \frac{\beta(y - \hat{y})}{(x - \hat{x})} \Leftrightarrow \hat{y} = y - \frac{(x - \hat{x})}{\beta}\eta.$$

Then y -integral is rewritten as

$$F(x, y, \hat{x}) = \int_{\eta^*}^1 \frac{1}{\beta} \sin(\lambda\hat{y}(\eta)) \frac{\cos\left(\zeta\sqrt{1-\eta^2}\right)}{\sqrt{1-\eta^2}} d\eta, \quad \zeta(x; \hat{x}) = \frac{\omega}{\beta^2}(x - \hat{x}).$$

In order to remove the singularity at $\eta = 1$, introduce one more variable:

$$\sin(\alpha) = \eta \Leftrightarrow \sqrt{1-\eta^2} = \cos(\alpha).$$

Then we finally obtain:

$$F(x, y, \hat{x}) = \int_{\alpha^*}^{\pi/2} \frac{1}{\beta} \sin(\lambda\hat{y}(\alpha)) \cos(\zeta \cos(\alpha)) d\alpha, \tag{21}$$

where

$$\alpha^*(x, y, \hat{x}) = \arcsin\left(\frac{\beta y}{x - \hat{x}}\right).$$

In this form the y -integral does not contain singularities and can be integrated by a regular integration rule.

With the given potential Φ_r (20) and (21), using expression for pressure (8), after long algebra we obtain $P_r(x, y)$ in the following form:

$$P_r(x, y) = -\mu \left(-i\omega\Phi_r(x, y) + M \frac{\partial\Phi_r(x, y)}{\partial x} \right) = \frac{\mu}{\pi} \int_0^{x_0} V(\hat{x})f(x, \hat{x})G(x, y, \hat{x})d\hat{x}, \tag{22}$$

where

$$G(x, y, \hat{x}) = \int_{\alpha^*}^{\pi/2} \left[\frac{i\omega}{\beta^3} \sin(\lambda\hat{y}(\alpha)) \cos(\zeta \cos(\alpha)) - \frac{\lambda M}{\beta} \sin(\alpha) \cos(\lambda\hat{y}(\alpha)) \cos(\zeta \cos(\alpha)) - \frac{\omega M}{\beta^2} \cos(\alpha) \sin(\lambda\hat{y}(\alpha)) \sin(\zeta \cos(\alpha)) \right] d\alpha. \tag{23}$$

Finally, consider the integral over the left small triangle $P_l(x, y)$. Since we consider deflections (17), where k and l are numbers of half-waves in x and y directions, respectively, it follows, due to symmetry for odd l and anti-symmetry for even l , that

$$P_l(x, y) = (-1)^{l+1} P_r(x, L_y - y).$$

3.3. Calculation of the aerodynamic force matrix

Now, consider the calculation of the integral (15) for a given pressure $P(x, y, T_m, \omega)$.

3.3.1. Series of plates

Let us first transform the expression (15), using (19). Let $T_m(x, y) = W_k(x)W^l(y)$ and $T_n(x, y) = W_r(x)W^s(y)$. After substitution of (19) into (15), the integral with respect to y is calculated in a closed form:

$$\begin{aligned} P_{nm}(\omega) &= \frac{2}{L_y} \int_0^{L_y} \int_0^{L_x} P(x, y, T_m, \omega) T_n(x, y) dx dy = \frac{2}{L_y} \int_0^{L_y} \int_0^{L_x} W^l(y) P_x(x, W_k(x), \omega) W_r(x) W^s(y) dx dy \\ &= \frac{2}{L_y} \int_0^{L_y} W^l(y) W^s(y) dy \int_0^{L_x} P_x(x, W_k(x), \omega) W_r(x) dx = \delta_i^s \int_0^{L_x} P_x(x, W_k(x), \omega) W_r(x) dx \end{aligned} \tag{24}$$

where δ_s^l is Kronecker delta.

It is seen that elements p_{nm} are non-zero only for $s=l$, which is satisfied when $[(m - 1)/N_x] = [(n - 1)/N_x]$. Hence, non-zero p_{nm} fill square blocks of the matrix P lying on the main diagonal.

For calculation of non-zero p_{nm} , we have to calculate two integrals with respect to x : outer (24), and inner (19). Both are calculated by the trapezoidal rule. When calculating the outer integral, we had q points per the shortest half-wave, i.e. the step size was

$$\Delta_x^{out} = \frac{L_x}{qN_x}$$

For calculation of the inner integral, we choose an r times smaller step size,

$$\Delta_x^{in} = \frac{\Delta_x^{out}}{r} = \frac{L_x}{rqN_x}$$

Values of N_x , r , and q are chosen based on the convergence study, which is conducted in Section 4.

Note that mode shapes of the plate in the flow along the x -axis (chordwise direction) are different from the mode shapes in vacuum, while they are not changed along the y (spanwise) direction and have a sinusoidal shape. Consequently,

$$\omega_i^j(D, \mu, L_x, L_y) = \omega_i^j\left(D, \mu, L_x, \frac{L_y}{j}\right), \tag{25}$$

where ω_i^j is the eigenfrequency corresponding to the mode (i, j) ; i and j are the numbers of half-waves of the eigenmode in the x and y directions, respectively. Thus, the instability boundary for the frequency with spanwise number $j > 1$ coincides with the instability boundary for the frequency with $j=1$ and accordingly changed L_y . Due to the same reason, in calculations it is enough to put $N_y=1$.

3.3.2. Single plate

In the case of a single plate, the outer integral (15) with respect to y cannot be computed in closed form, that is why it is also calculated numerically. Both integrals are calculated through the trapezoidal rule with uniform integration steps:

$$\Delta_x^{out} = \frac{L_x}{qN_x}, \quad \Delta_y^{out} = \frac{L_y}{qN_y}$$

For a single plate, pressure P consists of the same expression as for a series of plates, and subtracted pressures over left and right triangles. The component of pressure induced by the series of plates P_{series} is calculated just as described in Section 3.3.1. Subtracted quantity, $P_r(x; y)$ or $P_l(x; y)$, has a form of integral (22), which for each \hat{x} requires calculation of y -integral (23). They both are also calculated by the trapezoidal rule, but the step is generally m times smaller than for outer integrals:

$$\Delta_x^{lr} = \frac{\Delta_x^{out}}{m} = \frac{L_x}{mqN_x}, \quad \Delta_y^{lr} = \frac{\Delta_y^{out}}{m} = \frac{L_y}{mqN_y} \tag{26}$$

Note that since (23) is the integral in α , and the step size is uniform in y , it is not uniform in α , and each integration point is found as

$$\alpha_j = \alpha_j(x; y; \hat{x}_k; \hat{y}_l).$$

3.4. Method for solving the frequency equation

Consider the plate in vacuum. This case corresponds to the frequency equation (16) without the aerodynamic force matrix P :

$$\det\left(K - \frac{L_x \omega^2}{2} E\right) = 0. \tag{27}$$

This equation has N different real roots ω^2 , which correspond to natural frequencies in vacuum $\omega_{n0} = \sqrt{(2/L_x)k_{nn}}$. Negative frequencies are not considered, because eigenmotions for positive and negative frequencies coincide.

When aerodynamic forces are added, eigenfrequencies become complex, because the matrix $P(\omega)$ is non-symmetric and complex so that the system is non-conservative.

For the numerical solution of the frequency equation the following iterative procedure is used. For calculating the n -th eigenfrequency ω_n , we take the n -th natural frequency in vacuum $\omega_{n0} = \sqrt{(2/L_x)k_{nn}}$ as an initial approximation. Next, let us have the p -th approximation ω_{np} . We construct a matrix $A_{p+1}(\omega_{np}, \omega_{n(p+1)})$ so that it contains $\omega_{n(p+1)}$ in the simplest form. All its coefficients a_{ij} , except a_{nn} , are equal to the same coefficients of the matrix $A(\omega_{np})$, whereas a_{nn} is calculated as

$$a_{nn} = k_{nn} - \frac{L_x}{2}\omega_{n(p+1)}^2 + p_{nn}(\omega_{np}),$$

where k_{nn} and p_{nn} are coefficients of matrices K and P , respectively.

Thus, the equation for calculating $(p + 1)$ -th approximation $\omega_{n(p+1)}$ takes the form

$$\det A_{p+1}(\omega_{np}, \omega_{n(p+1)}) = 0. \tag{28}$$

It is linear with respect to $\omega_{n(p+1)}^2$; among two branches $\omega_{n(p+1)}$ we take the one with $\text{Re } \omega_{n(p+1)} > 0$.

Iterations for ω_n are continued until the relative inaccuracy becomes sufficiently small:

$$\left| \frac{\omega_{np} - \omega_{n(p-1)}}{\omega_{np}} \right| < \varepsilon. \tag{29}$$

According to the convergence study (Section 4), in calculations we used the value $\varepsilon = 10^{-4}$.

A modification of the iterative procedure is used for calculating frequencies $\omega_n = \omega_1^j$ and $\omega_{n+1} = \omega_2^j$ (as for basic functions, notation $\omega_m = \omega_k^l$ is used), which are responsible for the coupled-mode flutter. This type of flutter occurs when for certain parameters of the problem these two frequencies tend to each other in the complex plane. In this case the iterative procedure needs modification, because when iterations are close to the desired frequency, they can be cycled in form of ‘jumps’ of $\omega_{n(p+1)}$ from one frequency branch to the other (Fig. 4a). The modification solves this problem as follows. We construct the matrix $A_{p+1}(\omega_{np}, \omega_{n(p+1)})$ for the next approximation, where $\omega_{n(p+1)}$ is present in two elements:

$$a_{jj} = k_{jj} - \frac{L_x}{2}\omega_{n(p+1)}^2 + p_{jj}(\omega_{np}), \quad j = n, \quad n + 1. \tag{30}$$

Other coefficients a_{ij} of $A_{p+1}(\omega_{np}, \omega_{n(p+1)})$ are the same as of $A(\omega_{np})$. When solving the equation $\det A_{p+1}(\omega_{np}, \omega_{n(p+1)}) = 0$, we obtain four solutions, two of which, s_1 and s_2 , have positive real part. They correspond to frequencies ω_n and ω_{n+1} . The following rule chooses the root corresponding to the desired frequency. Let s_3 be a point lying in the centre of the segment connecting s_1 and s_2 in the complex plane, i.e., $s_3 = (s_1 + s_2)/2$ (Fig. 4b). Consider a line passing through s_3 and directed at the angle $\pi/4$ with respect to the real axis. Then the root lying above this line corresponds to the frequency ω_n , whereas the other root corresponds to the frequency ω_{n+1} . Thus, if $(\text{Im } s_1 - \text{Im } s_3) > (\text{Re } s_1 - \text{Re } s_3)$, then $s_1 = \omega_n$, $s_2 = \omega_{n+1}$, and vice versa.

4. Convergence study

Convergence was studied independently for both plate configurations. Since the eigenfrequency calculation for a single plate requires more numerical parameters, we will present results of the convergence study for this case only.

Analysis is conducted for parameters

$$D = 23.9, \quad \mu = 0.00012, \quad M = 1.2, \quad L_x = 300, \tag{31}$$

and various L_y .

First, we have studied the number of basic modes N_x, N_y . For the chordwise number N_x , calculations yield the result similar to

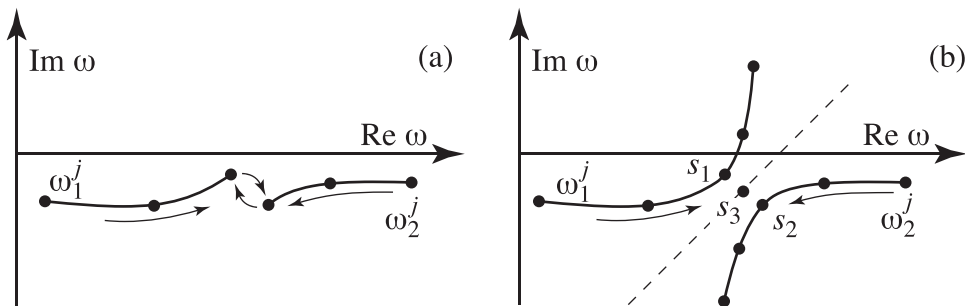


Fig. 4. Cycling of coalescing frequencies in the original method (a) and overcoming of the cycling by the modified method (b). Points represent frequency loci with iterations in the case of the coupled-mode flutter.

the two-dimensional case (Vedeneev, 2012): N_x equal to the highest frequency of interest gives the accurate solution. Namely, since the first four frequencies are calculated in this study, we computed the most representative pieces of flutter boundaries with $N_x = 4, \dots, 8$, and found that $N_x=4$ gives a well-converged results. This is naturally explained by the following. On one hand, the coupled-mode flutter boundary is formed by the coupling of the first two modes, and four basic functions give accurate results for these modes. On the other hand, single-mode flutter occurs due to negative aerodynamic damping of each mode, without significant influence of other modes. That is why the minimum number of modes is enough for accurate calculation of flutter boundaries, while the most important is the correct calculation of the aerodynamic damping.

Next, consider spanwise number of basic functions N_y . It was argued above that for the case of series of plates $N_y=1$ is enough, because mode shapes in the flow and in vacuum along the spanwise direction are not changes and thus normal to each other. However, for a single plate this is not the case. Calculations with $N_y = 2, \dots, 4$ show that flutter boundaries are almost unchanged, and $N_y=2$ is enough for accurate calculations.

Now, let us study the convergence in other parameters of the numerical procedure. We choose basic parameters $\epsilon = 10^{-4}$, $q=8$, $r=2$, and $m=2$. Then, a series of calculations with higher values of each parameter is conducted to ensure the convergence. Calculations are performed for the problem parameters (31) and $L_y = 1000, 500$, and 200.

Fig. 5 shows the convergence of real and imaginary parts of four frequencies, $\omega_1^i, \omega_2^i, \omega_3^i$, and ω_4^i in ϵ (29). Upper plots show real and imaginary parts of the frequencies, while bottom plots show their inaccuracies relative to the previous value of ϵ as:

$$\delta_{\text{Re}}(\epsilon) = \left| \frac{\text{Re } \omega(\epsilon) - \text{Re } \omega(10 \times \epsilon)}{\text{Re } \omega(\epsilon)} \right|, \quad \delta_{\text{Im}}(\epsilon) = \left| \frac{\text{Im } \omega(\epsilon) - \text{Im } \omega(10 \times \epsilon)}{\text{Im } \omega(\epsilon)} \right|. \tag{32}$$

In subsequent calculations we choose $\epsilon = 10^{-4}$, which yields satisfactory accuracy.

Next, consider convergence in the number of integration points q of the outer integral (15) per shortest half-wave taken into

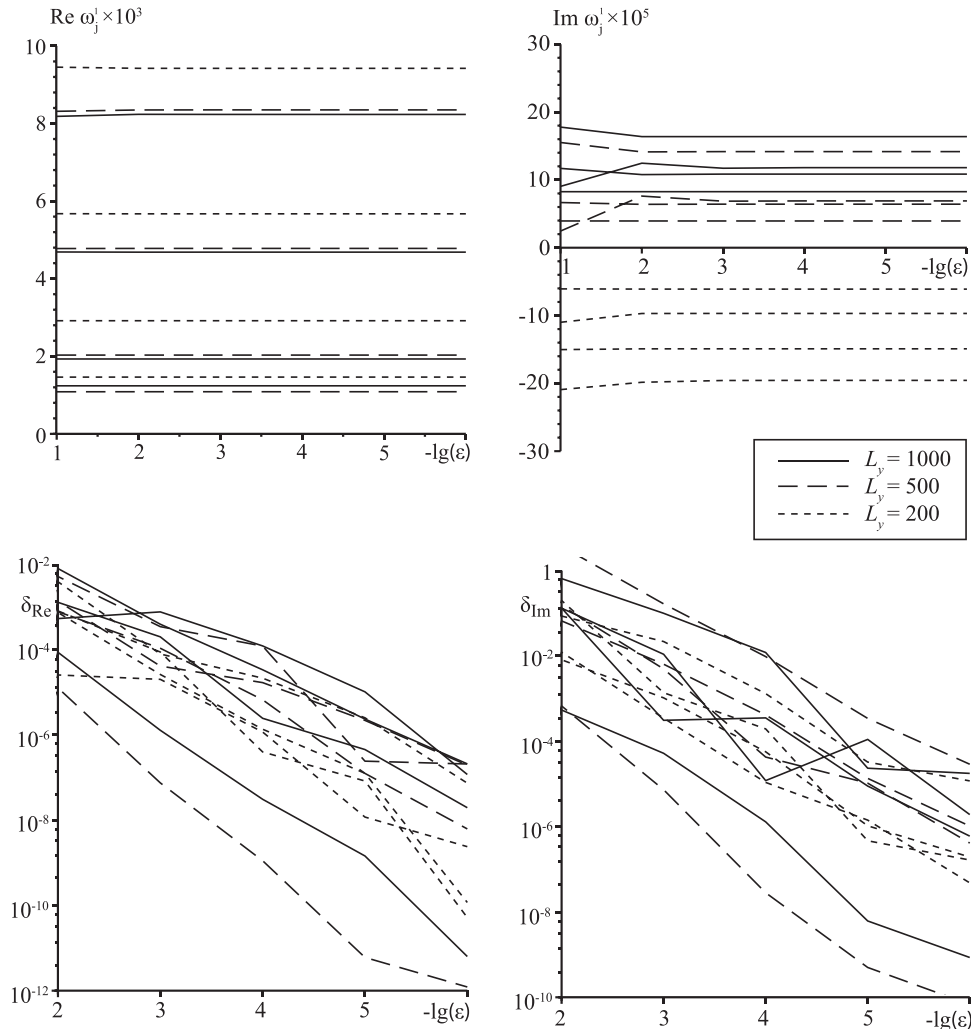


Fig. 5. Convergence in the relative inaccuracy ϵ . Frequencies $\omega_j^i, j = 1, \dots, 4$, and relative inaccuracies for parameters (31) and $L_y=200, 500$, and 1000 are shown.

account by the Bubnov–Galerkin method, shown in Fig. 6. The total number of points for calculating the outer integral is qN_x and qN_y , in the x and y directions, respectively. It is seen that $q=6$ is enough for obtaining accurate results.

Fig. 7 shows the convergence in the parameter r of the inner integral (19) calculation. Below we choose $r=3$, according to the results shown in Fig. 7.

Finally, shown in Fig. 8 is the convergence in the parameter m of calculating inner integrals over side triangles. We choose $m=3$, which, as can be seen, yields satisfactory accuracy.

As an illustration of the iterative process, Fig. 9a and b shows the convergence of the frequency ω_2^1 of a series of plates for $L_y=1000$ and 500 versus the iteration number p . Fig. 9c shows the value of $|\det A(\omega_2^1)|$ versus the iteration number. Note that, as described above, the iterations are finished when the condition (29) is satisfied, but additionally in each calculation it was checked that real and imaginary parts of the frequency tend to constant values, which is visually seen in Fig. 9. Similarly, the convergence was checked for other frequencies for various parameter values.

Based on the convergence study, we choose the following parameters of the numerical method: $N_x=4$, $N_y=2$, $q=6$, $r=3$, $m=3$, and $\epsilon = 10^{-4}$. These values are used below in calculations of the stability boundaries.

5. Results

Stability boundaries (i.e., level lines $\text{Im } \omega_j^1 = 0$) are calculated for the first four eigenfrequencies ω_j^1 ($j = 1, \dots, 4$) in the L_x – L_y – M space. All calculations are conducted for parameters

$$D = 23.9, \quad \mu = 0.00012, \tag{33}$$

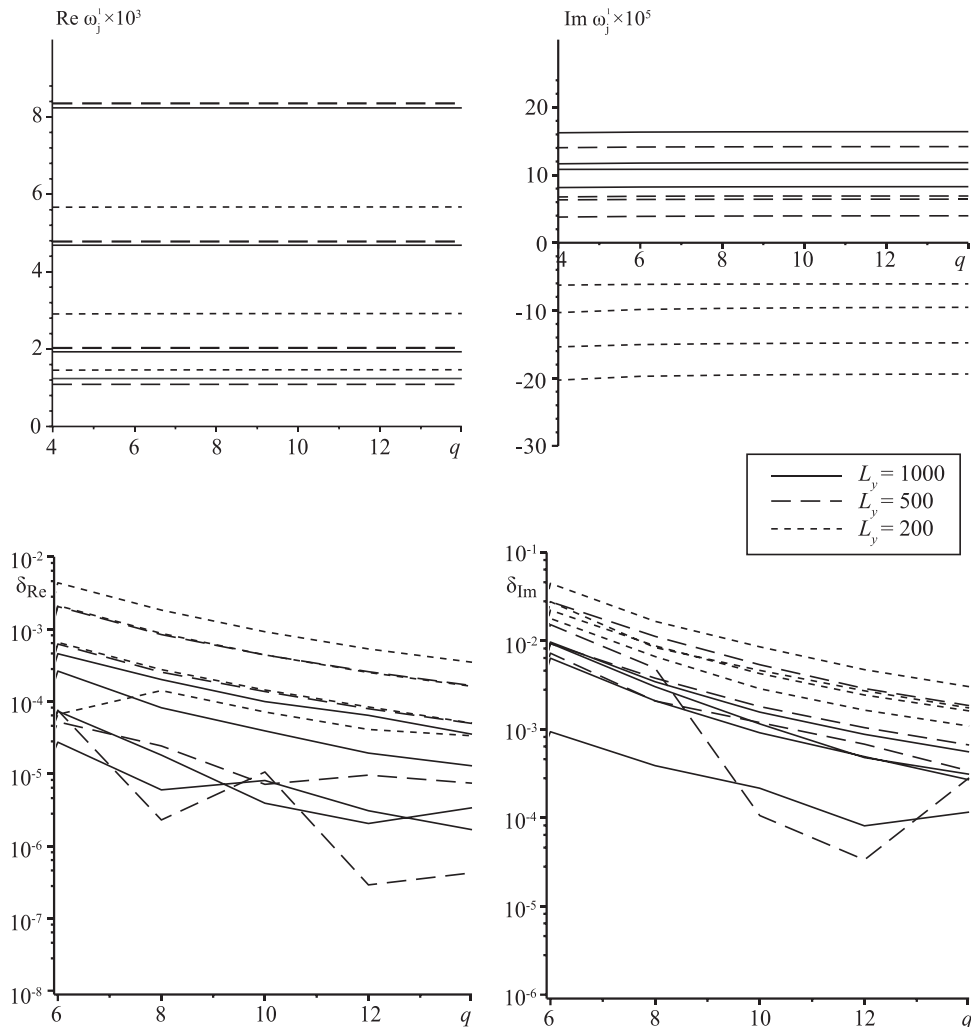


Fig. 6. Convergence in the parameter q governing calculation of the outer integral. Frequencies ω_j^1 , $j = 1, \dots, 4$, and relative inaccuracies for parameters (31) and $L_y=200, 500$, and 1000 are shown.

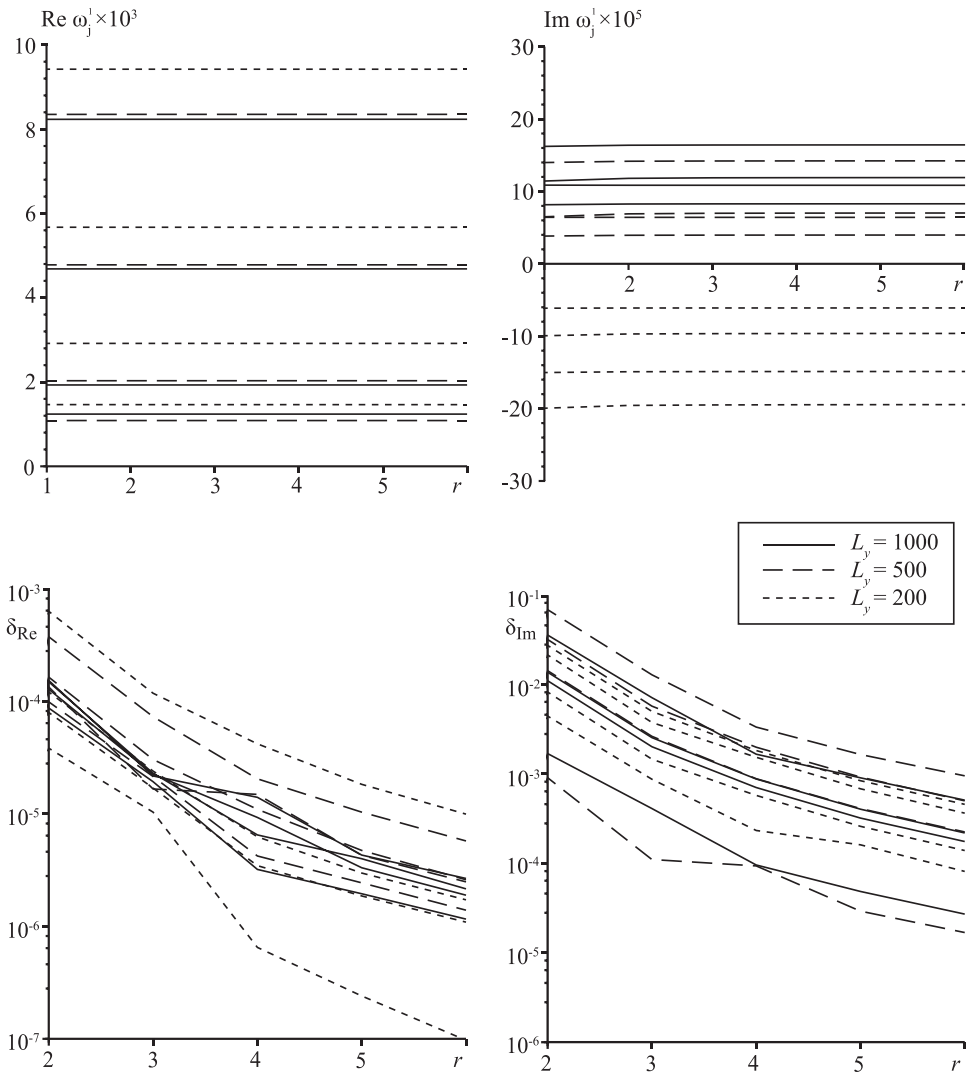


Fig. 7. Convergence in the parameter r governing calculation of the inner integral. Frequencies $\omega_j^1, j = 1, \dots, 4$, and relative inaccuracies for parameters (31) and $L_y=200, 500$, and 1000 are shown.

which correspond to a steel plate in an air flow at the altitude 3000 m above sea level. Aluminium plate at the altitude 11 000 m, where the air is more rarified, corresponds to close values $D=25.9, \mu = 0.00012$, so that parameters (33) can be considered as representative for this case too.

5.1. First mode flutter boundary

Consider the stability boundaries in the first mode (frequency ω_1^1), shown in the L_x-M plane in Fig. 10 for $L_y=1000, 500, 450, 400, 350$, and 300 . The region of $M < 1.5$ is shown. Solid curves represent series of plates, while dashed represent single plate. Maximum chordwise plate length L_{xmax} , at which the plate is stable for any spanwise widths L_y , equals to 57 and corresponds to $L_y = \infty$ (Vedeneev, 2012). It is seen that for $L_x > L_{xmax}$ and sufficiently large L_y there exists a segment $M^*(L_x, L_y) < M < M^{**}(L_x, L_y)$, in which the plate is unstable in the first mode. Note that stability boundaries for $L_y=1000$ for series of plates and single plate coincide with each other and almost coincide with the boundary calculated by Vedeneev (2012) in the two-dimensional formulation, i.e., for $L_y = \infty$. When spanwise width L_y decreases, the Mach number range, where the plate is unstable, narrows, and starting from a certain $L_y = L_{ys}$ the instability region is split into two isolated regions. The first, corresponding to smaller L_x , represents single mode flutter, while the second represents the coupled mode flutter. Fig. 11 shows the split in more details; the saddle point of the instability boundary at $L_{ys} \approx 425$ for the series of plates and at $L_{ys} \approx 356$ for single plate is clearly seen. When L_y is further decreased, the size of the single mode flutter region decreases and tends to the point $L_x \approx 92, M \approx 1.23$ for the series of plates, and $L_x \approx 95, M \approx 1.23$ for the single plate. For the series of plates, at $L_y=313$ the single mode flutter boundary is contracted to this point and

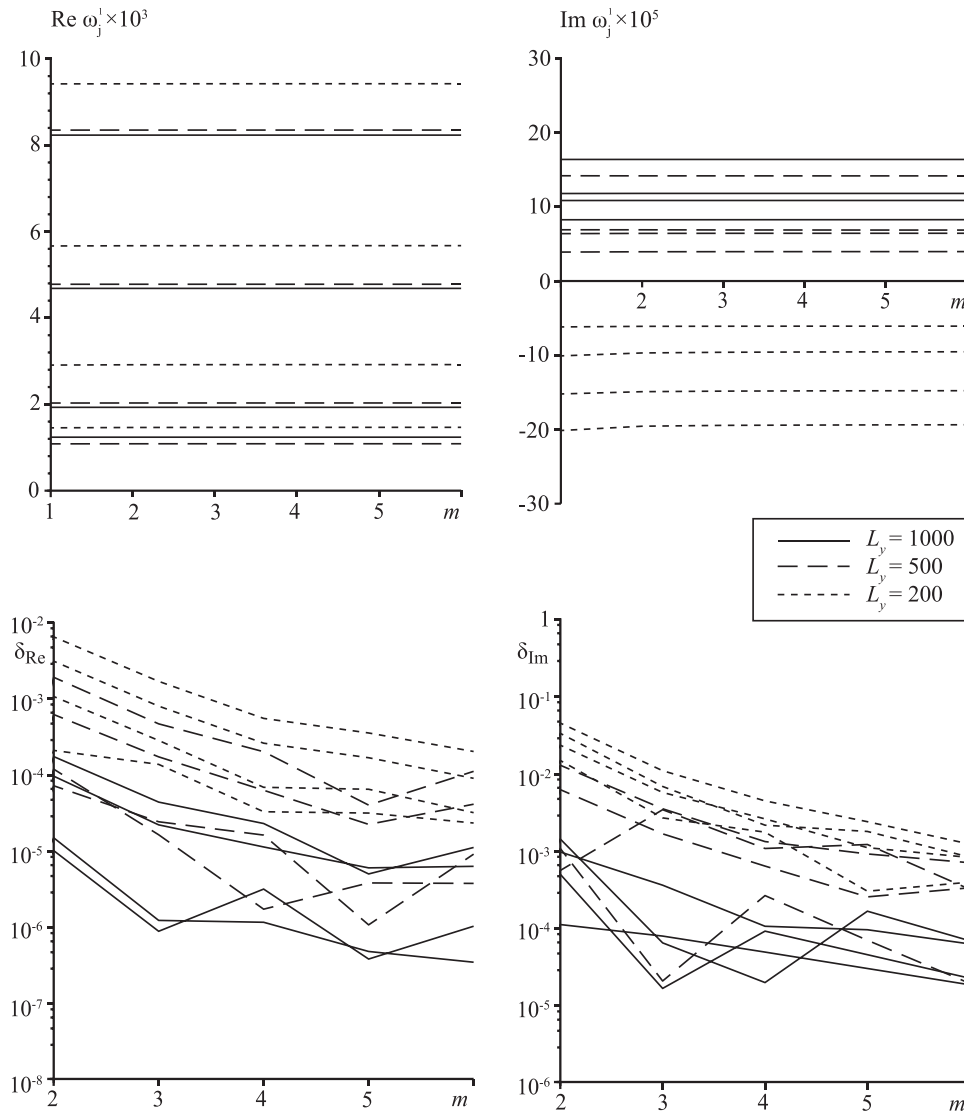


Fig. 8. Convergence in the parameter m governing calculation of integrals over small triangles. Frequencies $\omega_j^1, j = 1, \dots, 4$, and relative inaccuracies for parameters (31) and $L_y=200, 500$, and 1000 are shown.

disappears; for the single plate the contraction and disappearance occur at $L_y=291$. The coupled mode flutter boundary, when decreasing L_y , is changed much slower, moving to larger L_x .

Dotted curves in Fig. 10 represent stability boundaries, calculated through the piston theory, which can be obtained by neglecting the integral term in (19). It is seen that the single mode flutter region is absent, which is in agreement with asymptotic results (Vedeneev, 2005) and two-dimensional study (Vedeneev, 2012), whereas coupled mode flutter boundaries, calculated through the piston and potential flow theories, become close to each other when decreasing L_y .

Fig. 12 shows flutter boundaries in the range $1.5 < M < 5.0$ for the same values of L_y . Results for series of plates and single plate are almost identical. Calculations through the piston theory are shown by dotted curves. It is seen that single mode flutter in the first mode is absent at these Mach numbers, whereas coupled mode flutter boundaries obtained through potential flow and piston theories almost coincide.

5.2. Higher modes

Now, consider results for higher modes. Fig. 13 shows flutter region in the second mode (frequency ω_2^1) at $L_y=1000, 400, 300, 250$, and 200 . These regions are bounded from the right by values of L_x , at which coupled mode flutter occurs: the first mode becomes growing, and the second becomes damped. As for the first mode, the decrease of L_y yields the compression of the single

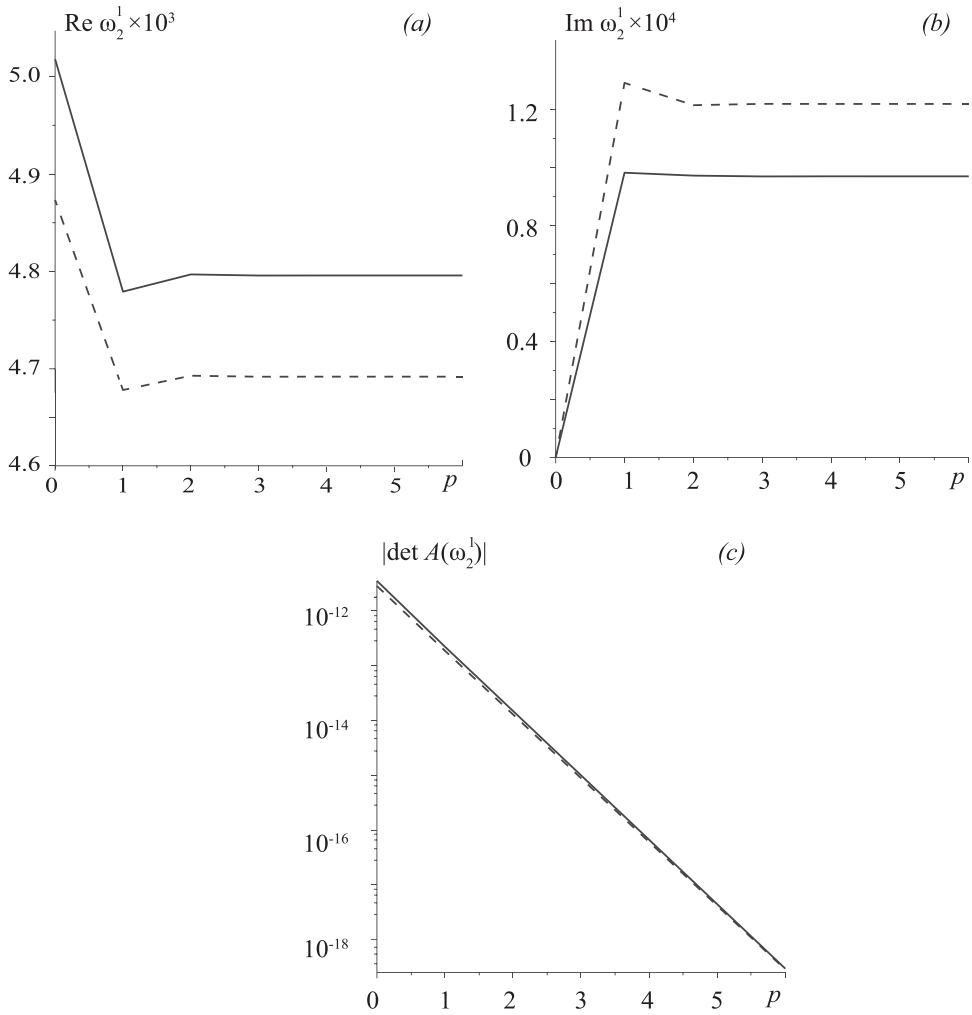


Fig. 9. Frequency ω_2^1 (a and b), $|\det A(\omega_2^1)|$ (c) versus the iteration number p at $L_y=1000$ (dashed curves) and 500 (solid curves).

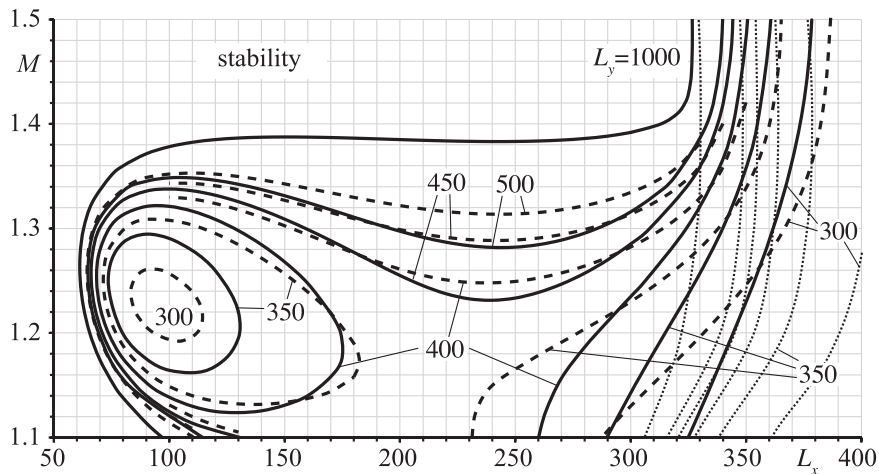


Fig. 10. Stability boundaries of the mode (1,1) (frequency ω_1^1) in the L_x - M plane for various L_y at $1.1 < M < 1.5$. Series of plates (solid curves) and single plate (dashed curves). Boundaries obtained through the piston theory are shown by dotted curves.

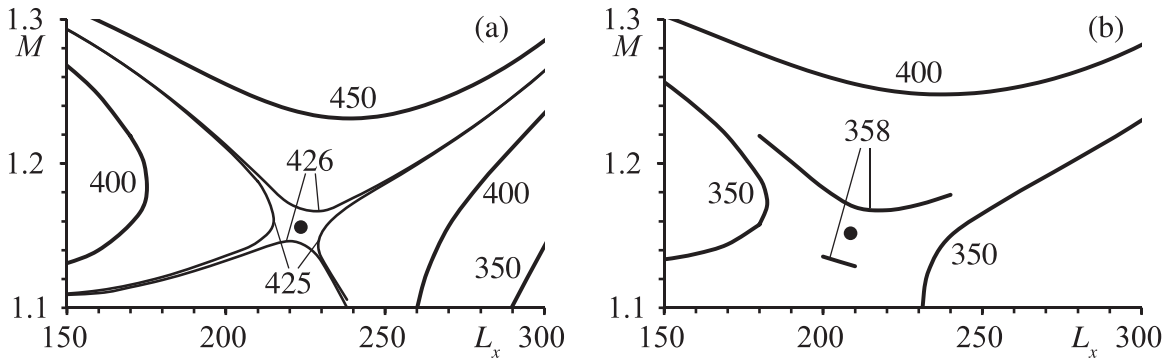


Fig. 11. Stability boundaries of the mode (1,1) in the L_x - M plane for L_y near the split of the single mode and coupled mode flutter boundaries. Series of plates (a) and single plate (b). Saddle point of the instability boundary is shown by the circle.

mode flutter region. At $L_y \approx 174$ (series of plates), and $L_y \approx 185$ (single plate) it is contracted to the point $L_x \approx 130, M \approx 1.41$ (series of plates), and $L_x \approx 129, M \approx 1.37$ (single plate), and disappears for lower L_y .

In contrast to the first two modes, flutter boundaries in the 3rd and the 4th modes, which do not take part in the generation of the coupled mode flutter, for $L_y = \infty$ have asymptotes $M^* = 1, M^{**} = \sqrt{2}$ as $L_x \rightarrow \infty$ (Vedeneev, 2012) (Figs. 14 and 15, respectively). Flutter boundaries at $L_y=1000$ are very close to those of the two-dimensional problem. When L_y decreases, their behaviour is different for the two plate configurations. In the case of a series of plates, flutter boundaries are shifted to higher M and become bounded in L_x direction. Further, as for single mode flutter in the first two modes, flutter boundaries are contracted to certain points and disappear. For the 3rd mode, the flutter region disappears at $L_y \approx 105$, and the boundary is contracted to the point $L_x \approx 177, M \approx 1.6$. Similarly, the instability region of the 4th mode disappears at $L_y \approx 79$, and its boundary is contracted to the point $L_x \approx 200, M \approx 1.73$.

In the case of a single plate, flutter regions also become bounded, but they are ‘embedded’ inside of each other (Figs. 14 and 15), and Mach numbers corresponding to instability do not grow when L_y decreases. Flutter region in the 3rd mode disappears at $L_y \approx 131$, and the boundary is contracted to the point $L_x \approx 153, M \approx 1.47$. Instability region in the fourth mode disappears at $L_y \approx 111$, and its boundary is contracted to the point $L_x \approx 170, M \approx 1.53$.

5.3. Comparison with other studies

First, let us compare these results with Movchan’s solution, given by formula (3.8) of Movchan (1957), which after

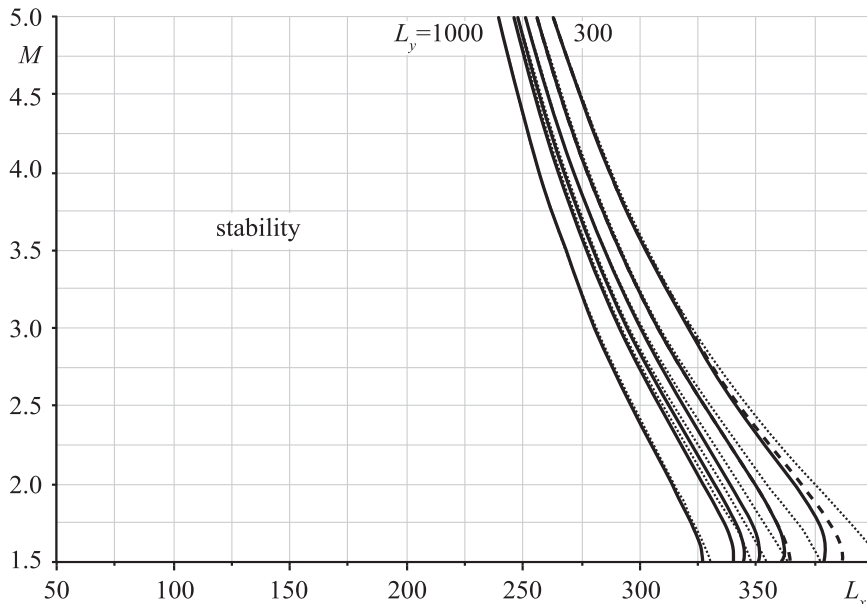


Fig. 12. Stability boundaries of the mode (1,1) in the L_x - M plane for various L_y at $1.5 < M < 5.0$. Series of plates (solid curves) and single plate (dashed curves); for $L_y > 350$ the curves for both cases coincide. Boundaries obtained through the piston theory are shown by dotted curves.

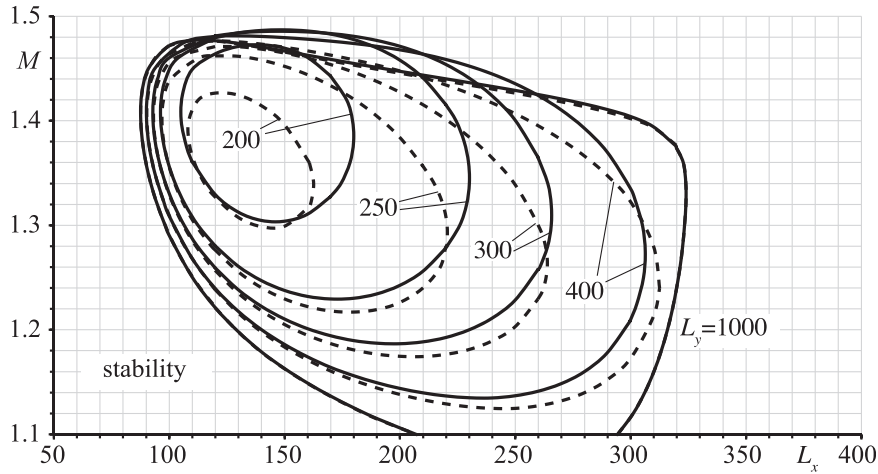


Fig. 13. Stability boundaries of the mode (2,1) (frequency ω_2^1) in the L_x - M plane for various L_y . Series of plates (solid curves) and single plate (dashed curves).

nondimensionalisation is written in the following form:

$$M = \frac{D}{\mu L_x^3} \frac{8\pi^3}{3\sqrt{3}} \left(5 + \left(\frac{L_x}{L_y} \right)^2 \right) \sqrt{2 + \left(\frac{L_x}{L_y} \right)^2}. \tag{34}$$

He used the piston theory in the form

$$p = \mu \left(M \frac{\partial w}{\partial x} + \frac{\partial w}{\partial t} \right). \tag{35}$$

Modification of the piston theory, which is more suitable for $M < 3$, has an additional multiplier $M/\sqrt{M^2 - 1}$, i.e.

$$p = \frac{\mu M}{\beta} \left(M \frac{\partial w}{\partial x} + \frac{\partial w}{\partial t} \right). \tag{36}$$

Assuming that the aerodynamic damping does not essentially influence the coupled mode flutter, the boundary obtained through this modification is derived from (34) by changing M to $M^2/\sqrt{M^2 - 1}$ in the left-hand side. Formula (36) is restored by the present method when neglecting the integral term in (19) and was used in a special series of calculations.

Fig. 16 shows original and modified flutter boundaries (34) (dashed and dash-and-dot curves), and flutter boundaries calculated by the present method by using the piston and potential flow theories (dotted and solid curves) for the first mode. Calculations are conducted for a series of plates for $L_y=350$ and 1000. It is seen that at high Mach numbers, $M > 3$, all four theories yield the same

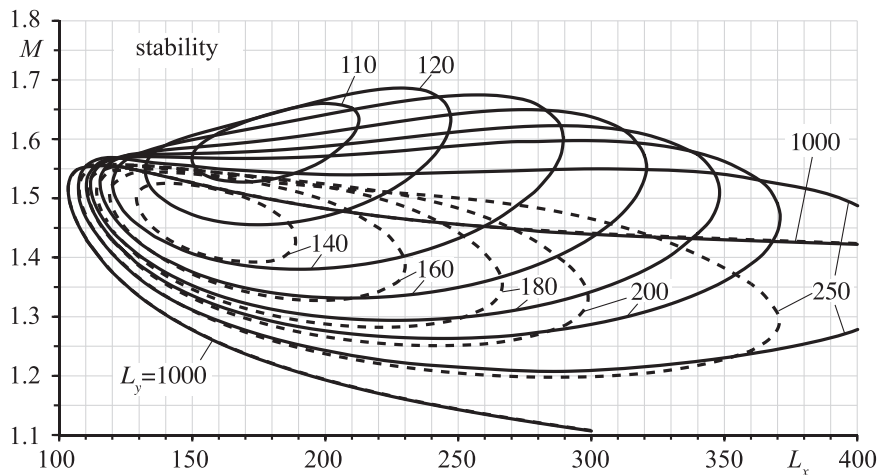


Fig. 14. Stability boundaries of the mode (3,1) (frequency ω_3^1) in the L_x - M plane for various L_y . Series of plates (solid curves) and single plate (dashed curves).

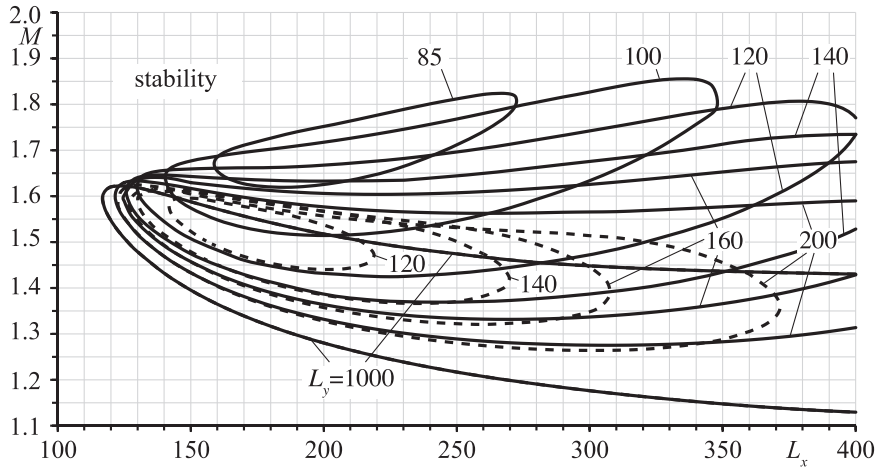


Fig. 15. Stability boundaries of the mode (4,1) (frequency ω_4^1) in the L_x - M plane for various L_y . Series of plates (solid curves) and single plate (dashed curves).

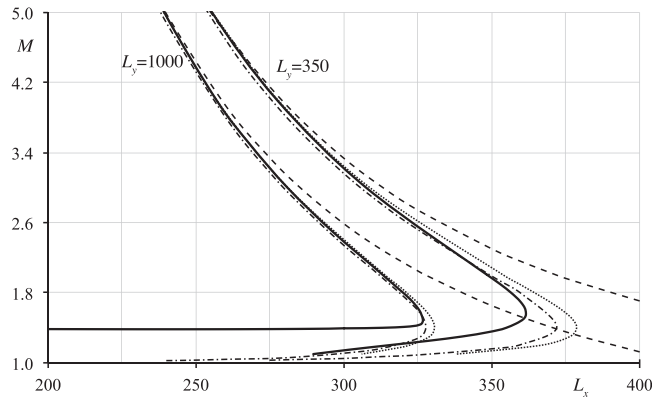


Fig. 16. Comparison of flutter boundaries in the first mode obtained by the potential flow theory (series of plates, solid curves) and several versions of the piston theory: Movchan's boundary (34), its modification, and results of the present study obtained through the piston theory (36) (dashed, dash-and-dot, and dotted curves, respectively).

results. For $M < 3$, the original version of the piston theory used by Movchan (1957), gives a significant inaccuracy. However, the modified version is accurate down to $M \approx 1.6$. At lower M , the piston theory is not applicable for calculation of the first mode flutter boundary because it is not able to predict the single mode flutter, which yields significant enlargement of the instability boundary in the first mode. For the flutter in higher modes, the piston theory does not yield instability, and thus is never applicable, since flutter in such modes is always of single-mode type, except for the case of plates essentially elongated in the flow direction, when the coupled mode flutter occurs not in the first, but in higher mode.

Next, let us compare results of the present study with those of Cunningham (1967), who calculated flutter boundaries at $M=1.3$ through the potential flow theory for different ratios L_x/L_y . He used different dimensionless parameters and plotted flutter boundaries in the plane $1/\mu^* - \omega_1^* l^*/V^*$, where asterisks represent the parameters of Cunningham (1967), which are expressed through the parameters of the present study as follows:

$$1/\mu^* = \frac{\rho_0 L_{xw}}{\rho_n h} = \mu L_x, \quad \omega_1^* l^*/V^* = \pi^2 \sqrt{\frac{D_w}{\rho_n h L_{xw}^4}} \left(1 + \left(\frac{L_{xw}}{L_{yw}} \right)^2 \right) \frac{L_{xw}}{U_0} = \pi^2 \frac{\sqrt{D}}{M L_x} \left(1 + \left(\frac{L_x}{L_y} \right)^2 \right).$$

His Fig. 3a–d shows flutter boundaries in the first four modes, which are reproduced as solid curves in Fig. 17. Our parameters (33) correspond to the dashed curve in Fig. 17. Flutter boundaries at the condition of a given L_x/L_y ratio, found from Figs. 10, and 13–15, are shown in Fig. 17 by symbols. It can be seen that in all cases the symbols are located very close to the intersection of solid and dashed curves; i.e., the correlation between Cunningham (1967) and the present study is very good. For the case of $L_x/L_y = 1/2$, he does not have the 3rd and 4th mode boundaries plotted, and for $L_x/L_y = 1$ he does not have the 4th mode boundary; those boundaries probably were not noticed in his calculations.

The results of this study explain why the order of the first mode flutter boundary is changed compared to other modes boundaries in Cunningham's Fig. 3 (our Fig. 17) when L_x/L_y ratio is increased. This occurs because for small L_x/L_y , the point is located at the left piece of the boundary shown in Fig. 10. When L_x/L_y is increased, the point moves to higher L_x in Fig. 10, being close to the coupled-

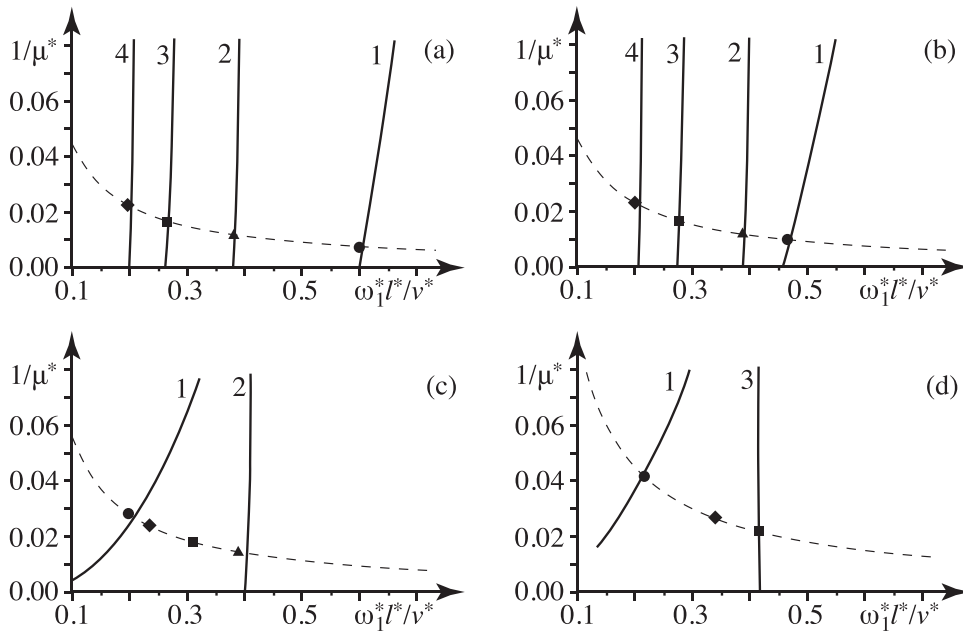


Fig. 17. Comparison of the single mode flutter boundaries with the results obtained by Cunningham (1967). His data are shown by solid curves (from his Fig. 3a–d); numbers denote the eigenmode number of each boundary. Dashed curves represent the parameters (33). Results of the present study are shown as symbols for the first (•), second (▲), third (■), and fourth (◆) mode. $L_x/L_y = 0$ (a), $1/4$ (b), $1/2$ (c), and 1 (d).

mode flutter boundary.

Finally, let us compare results with the asymptotic theory of single mode flutter (Vedeneev, 2006), which will explain the shift of single mode flutter regions to higher Mach numbers when L_y decreases in the case of the series of plates. When the plate length and width L_x, L_y are large, eigenmodes can be represented as cycled reflections of travelling waves from the plate edges (Kulikovskii, 2006). The criterion of the eigenmode growth depends on the angle between the wave vector and the flow direction. The decrease of L_y yields the increase of this angle, which leads to the increase of Mach numbers where the eigenmode is amplified. Quantitatively, the results of Vedeneev (2006) yield the following single mode flutter boundaries $M^*(L_x, L_y) < M < M^{**}(L_x, L_y)$ for large plates:

$$M^* = \sqrt{1 + \left(\frac{n}{m}\right)^2 \left(\frac{L_x}{L_y}\right)^2} (1 + \sqrt{Dk_0^2}), M^{**} = \sqrt{1 + \left(\frac{n}{m}\right)^2 \left(\frac{L_x}{L_y}\right)^2} \sqrt{1 + Dk_0^2 + \sqrt{4Dk_0^2 + 1}}, \tag{37}$$

where m and n are the numbers of half-waves in the x and y directions, and

$$k_0 = \sqrt{(m\pi/L_x)^2 + (n\pi/L_y)^2}.$$

Fig. 18 shows the comparison of boundaries obtained numerically (thick curves) and through asymptotic formulae (37) (thin curves). Fig. 18a shows flutter boundaries in the 3rd mode for $L_y=1000, 200, 130,$ and 110 (solid, dashed, dash-and-dot, and dotted curves). Fig. 18b shows the same boundaries for the 4th mode for $L_y=1000, 200, 100,$ and 82 . As can be seen, the increase of Mach numbers in the ‘central’ part of the flutter boundary, $L_x = 100 \dots 300$, is correctly captured by the asymptotic solution. The difference is significant at small L_x , where the condition of large plate lengths in the x -direction is not satisfied, and at large M , which are achieved only at sufficiently small L_y so that the condition of large plate width in the y -direction is broken.

Thus, the asymptotic theory of Vedeneev (2006) explains the shift to higher M of single mode flutter boundaries in the third and fourth modes in the case of series of plates. Apparently, in the case of the single plate, the absence of this shift is due to different aerodynamics, which is not taken into account by the asymptotic theory.

6. Conclusions

In this paper we numerically investigated flutter boundaries of a simply supported rectangular plate in the first four eigenmodes through potential flow aerodynamics. Two plate configurations are considered: series of plates oscillating simultaneously, and a single plate. While for a two-dimensional plate ($L_y = \infty$) the first mode flutter boundary consists of single mode and coupled mode flutter boundaries attached to each other, for small L_y it is split into two isolated flutter regions in the parameter space. For sufficiently small L_y , single mode flutter boundaries for the first two eigenmodes contract to a point and disappear, whereas a coupled mode flutter boundary remains and moves to higher plate lengths L_x .

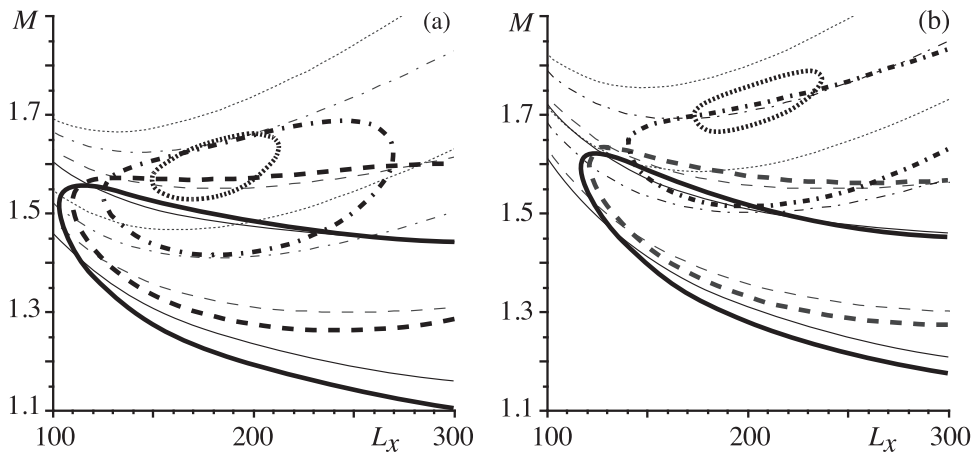


Fig. 18. Comparison of the calculated flutter boundaries in the 3rd (a) and 4th (b) modes (thick curves) with asymptotic formulae (37) (thin curves).

For the third and the fourth modes of the series of plates, the decrease of L_y yields the shift of the single mode flutter boundary to higher M , which is explained by the asymptotic theory for long plates. For a single plate the shift to higher M is absent, which is a consequence of the different aerodynamics of series of plates and a single plate.

Results of the present paper can be used directly in the design of skin panels for flight vehicles. Also, they provide important information on the linear growth mechanism, which is significant in the analysis of nonlinear limit cycle oscillations. In particular, the split of the instability boundary of the first mode for $L_x < 356$ allows using the operating zone in the gap of stability at $170 < L_x < 250$, where the first mode is damped.

Acknowledgement

This work is supported by the Russian Science Foundation under grant 14-50-00005.

References

- Alder, M., 2015. Development and validation of a fluid–structure solver for transonic panel flutter. *AIAA J.* 53 (12), 3509–3521.
- Alder, M., 2016. Nonlinear dynamics of pre-stressed panels in low supersonic turbulent flow. *AIAA J.* 54 (11), 3632–3646.
- Ashley, H., Zartarian, G., 1956. Piston theory – a new aerodynamic tool for the aeroelastician. *J. Aeronaut. Sci.* 23 (12), 1109–1118.
- Algazin, S.D., Kiiko, I.A., 2006. Flutter of plates and shells. *Nauka, Moscow* (in Russian. Translated in Algazin, S.D., Kijko, I.A., 2014. *Aeroelastic Vibrations and Stability of Plates and Shells. De Gruyter Studies in Mathematical Physics*, vol. 25. Walter de Gruyter, Berlin).
- Bendiksen, O.O., Davis, G.A., 1995. Nonlinear Traveling Wave Flutter of Panels in Transonic Flow. *AIAA Paper* 95-1486.
- Bendiksen, O.O., Seber, G., 2008. Fluid–structure interactions with both structural and fluid nonlinearities. *J. Sound Vib.* 315 (3), 664–684.
- Bolotin, V.V., 1963. *Nonconservative Problems of the Theory of Elastic Stability*. Pergamon Press, Oxford.
- Bondarev, V.O., Vedeneev, V.V., 2016. Short-wave instability of an elastic plate in supersonic flow in the presence of the boundary layer. *J. Fluid Mech.* 802, 528–552.
- Cunningham, H.J., 1967. Flutter Analysis of Flat Rectangular Panels Based in Three-Dimensional Supersonic Unsteady Potential Flow. *NASA Technical Report No. R-256*.
- Dowell, E.H., 1971. Generalized aerodynamic forces on a flexible plate undergoing transient motion in a shear flow with an application to panel flutter. *AIAA J.* 9 (5), 834–841.
- Dowell, E.H., 1973. Aerodynamic boundary layer effect on flutter and damping of plates. *J. Aircr.* 10 (12), 734–738.
- Dowell, E.H., 1974. *Aeroelasticity of Plates and Shells*. Northhoff International Publishing, Leyden.
- Duan, B., Abdel-Motagaly, K., Guo, X., Mei, C., 2003. Suppression of Supersonic Panel Flutter and Thermal Deflection Using Shape Memory Alloy. *AIAA Paper* 1513-2003.
- Dugundji, J., 1966. Theoretical considerations of panel flutter at high supersonic Mach numbers. *AIAA J.* 4 (7), 1257–1266.
- Ganji, H.F., Dowell, E.H., 2016. Panel flutter prediction in two dimensional flow with enhanced piston theory. *J. Fluids Struct.* 63, 97–102.
- Gordnier, R.E., Visbal, M.R., 2002. Development of a three-dimensional viscous aeroelastic solver for nonlinear panel flutter. *J. Fluids Struct.* 16 (4), 497–527.
- Grigolyuk, E.I., Lamper, R.E., Shandarov, L.G., 1965. Flutter of plates and shells. In: *Itogi Nauki. Mekhanika*. 1963. VINITI, Moscow, pp. 34–90 (in Russian).
- Hashimoto, A., Aoyama, T., Nakamura, Y., 2009. Effect of turbulent boundary layer on panel flutter. *AIAA J.* 47 (12), 2785–2791.
- Iliushin, A.A., 1956. Plane section law in the high-speed aerodynamics. *Prikl. Mat. Mek.* 20 (6), 733–755, (in Russian).
- Kiiko, I.A., Pokazeev, V.V., 2005. Vibrations and stability of a viscoelastic strip placed into gas flow. *Dokl. Phys.* 50 (3), 158–160.
- Kulikovskii, A.G., 1966. On the stability of homogeneous states. *J. Appl. Math. Mech.* 30 (1), 180–187.
- Kulikovskii, A.G., 2006. The global instability of uniform flows in non-one-dimensional regions. *J. Appl. Math. Mech.* 70 (2), 229–234.
- Min-de, Dun, 1958. On the stability of elastic plates in a supersonic stream. *Sov. Phys. Dokl.* 3, 479–482.
- Ming-de, Dong, 1984. Eigenvalue problem for integro-differential equation of supersonic panel flutter. *Appl. Math. Mech.* 5 (1), 1029–1040.
- Mei, C., Abdel-Motagaly, K., Chen, R.R., 1999. Review of nonlinear panel flutter at supersonic and hypersonic speeds. *Appl. Mech. Rev.* 10, 321–332.
- Mei, G., Zhang, J., Xi, G., Sun, X., Chen, J., 2014. Analysis of supersonic and transonic panel flutter using a fluid–structure coupling algorithm. *J. Vib. Acoust.* 136, 031013.
- Miles, J.W., 1959. *The Potential Theory of Unsteady Supersonic Flow*. Cambridge University Press, Cambridge.
- Movchan, A.A., 1956. On oscillations of a plate moving in a gas. *Prikl. Mat. Mek.* 20 (2), 211–222, (in Russian).
- Movchan, A.A., 1957. On stability of a panel moving in a gas. *Prikl. Mat. Mek.* 21 (2), 231–243, (in Russian. Translated in NASA RE 11-22-58 W, 1959).
- Nelson, H.C., Cunningham, H.J., 1956. Theoretical Investigation of Flutter of Two-Dimensional Flat Panels With One Surface Exposed to Supersonic Potential Flow. *NACA Report No. 1280*.

- Novichkov, Yu.N., 1978. Flutter of plates and shells. In: *Progress in Science and Technology. Mechanics of Deformable Solids*, vol. 11. VINITI, Moscow, pp. 67–122 (in Russian).
- Shishaeva, A., Vedeneev, V., Aksenov, A., 2015. Nonlinear single-mode and multi-mode panel flutter oscillations at low supersonic speeds. *J. Fluids Struct.* 56, 205–223.
- Vedeneev, V.V., 2005. Flutter of a wide strip plate in a supersonic gas flow. *Fluid Dyn.* 5, 805–817.
- Vedeneev, V.V., 2006. High-frequency flutter of a rectangular plate. *Fluid Dyn.* 4, 641–648.
- Vedeneev, V.V., 2007. Nonlinear high-frequency flutter of a plate. *Fluid Dyn.* 5, 858–868.
- Vedeneev, V.V., 2010. Study of the single-mode flutter of a rectangular plate in the case of variable amplification of the eigenmode along the plate. *Fluid Dyn.* 45 (4), 656–666.
- Vedeneev, V.V., 2012. Panel flutter at low supersonic speeds. *J. Fluids Struct.* 29, 79–96.
- Vedeneev, V.V., 2013a. Effect of damping on flutter of simply supported and clamped panels at low supersonic speeds. *J. Fluids Struct.* 40, 366–372.
- Vedeneev, V.V., 2013b. Limit oscillatory cycles in the single mode flutter of a plate. *J. Appl. Math. Mech.* 77 (3), 257–267.
- Vedeneev, V.V., 2013c. Interaction of panel flutter with inviscid boundary layer instability in supersonic flow. *J. Fluid Mech.* 736, 216–249.
- Visbal, M., 2014. Viscous and inviscid interactions of an oblique shock with a flexible panel. *J. Fluids Struct.* 48, 27–45.
- Yang, T.Y., 1975. Flutter of flat finite element panels in supersonic potential flow. *AIAA J.* 13 (11), 1502–1507.
- Zhou, R.C., Lai, Z., Xue, D.Y., Huang, J.-K., Mei, C., 1995. Suppression of nonlinear panel flutter with piezoelectric actuators using finite element method. *AIAA J.* 33 (6), 1098–1105.